ANALYSIS OF VIBRATORY STRESS OF INTEGRAL SHROUD BLADE FOR MECHANICAL DRIVE STEAM TURBINE

by

Yasutomo Kaneko

Senior Research Engineering Manager

Kazushi Mori

Chief Research Engineer

Toshihiro Miyawaki

Senior Research Engineer

Mitsubishi Heavy Industries, Ltd.,

Hyogo, Japan

and

Satoshi Hata

Group Manager, Turbo Machinery Engineering Department

Mitsubishi Heavy Industries, Ltd.,

Hiroshima, Japan

Yasutomo Kaneko is a Senior Research Engineering Manager in Takasago Research & Development Center, Mitsubishi Heavy Industries, Ltd., in Hyogo, Japan. He is a turbomachinery specialist in the area of vibration. He has 25 years of experience in the field of rotordynamics, specializing in the field of blade vibration.

Dr. Kaneko has B.S., M.S., and Ph.D. degrees (Mechanical Engineering) from Hokkaido University.

Kazushi Mori is a Chief Research Engineer in Takasago Research & Development Center, Mitsubishi Heavy Industries, Ltd., in Hyogo, Japan. He is a specialist in the area of blade vibration with 12 years of experience.

Mr. Mori has B.S. and M.S. degrees (Mechanical Engineering) from Kyoto University.

Toshihiro Miyawaki is a Senior Research Engineer in Takasago Research & Development Center, Mitsubishi Heavy Industries, Ltd., in Hyogo, Japan. He is an aerodynamics specialist and has 20 years of experience with R&D of steam turbine blade designs.

Mr. Miyawaki has B.S. and M.S. degrees (Mechanical Engineering) from Osaka University.

ABSTRACT

The advanced integral shroud blade (ISB) structure has been developed to improve the reliability and thermal efficiency of mechanical drive steam turbines. This advanced ISB has been applied to not only the control stage blades but also the intermediate stage blades. Turbines using these advanced blades have been successfully operated.

This paper presents the analysis method to calculate the vibratory stresses of the ISB caused by the stage interaction force and the shock load. The vibration response characteristics are explained and comparisons are made to the advanced ISB structure and the conventional grouped blade structure, using the calculated results. Additional verification test results to confirm the validity of the proposed analysis method are also shown.

INTRODUCTION

In order to improve the reliability and thermal efficiency of mechanical drive steam turbines, advanced blade designs have been developed (Ikeno, et al., 2004). The advanced blade designs are typified by the integral shroud blade (ISB) structure. With this design, the blades are continuously coupled by blade deformation due to centrifugal force. Because the twist back deformation of the intermediate and control stage blades is very small, the innovative mechanism of the advanced ISB differs from the well-known blade untwist effect and is used to induce contact with adjacent blades. This advanced ISB has been applied to not only the control stage blades but also the intermediate stage blades, and all the turbines using the advanced blades have exhibited successful operation.

In order to develop the advanced blades, analysis methods predicting the vibration characteristics of the ISB structure were developed, and their validity was confirmed before applying them to the blade design. In this paper, the analysis methods to predict the vibratory stress of the ISB and their applications are described.

Generally, in designing the ISB for a mechanical steam turbine, two types of excitation forces should be considered. One is the

stage interaction force between blades and vanes. Another is the shock load due to partial admission operation of the control stage. In predicting the vibratory stress caused by these excitation forces, the unsteady fluid dynamics using a computational fluid dynamics (CFD) model and the modal analysis based on the finite element analysis (FEA) were studied.

In this paper, the analysis method to calculate the vibratory stress of the blades caused by the stage interaction force and the shock load is presented first. Second, the vibration response characteristics are explained and compared for the advanced ISB structure and conventional grouped blade structure, using the calculated results. Some verification test results to confirm the validity of the proposed analysis method are also shown. Finally, the successful field experiences of steam turbines using the advanced ISB design are described.

FEATURE OF ADVANCED INTEGRAL SHROUD BLADE

In the intermediate and control stages of mechanical steam turbines, parallel and short blades are used. The conventional ISB structure that is normally applied to long twisted blades, where the blades are continuously coupled at the adjacent shrouds by virtue of untwist deformation, cannot be applied. This is because the untwist deformation of the parallel and short blades due to centrifugal force is very small. In this case, the advanced ISB structure shown in Figure 1 applies an innovative design to induce contact with adjacent blades.

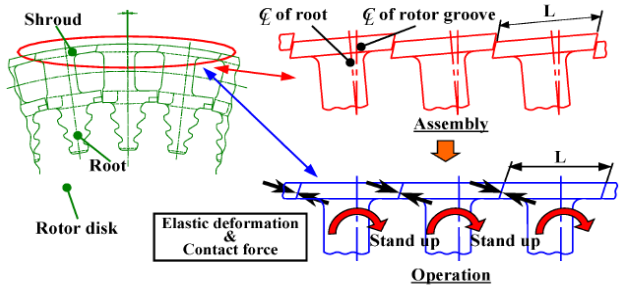

Figure 1. Advanced ISB Structure.

In the advanced ISB structure shown in Figure 1, the length of the shroud pitch, L, is designed to be slightly longer than the nominal pitch as determined by the shroud radius and the number of blades. In assembling the disk, each blade is inserted into the groove on the slant by use of the clearance between the root and groove. In rotation, the blades are continuously coupled at the shrouds by virtue of the moment induced by the centrifugal force. This makes the blade rise from the slant position. In this mechanism, if the increment of the shroud pitch is designed to be bigger than the increment of shroud gap due to centrifugal force and thermal deformation in operation, the blade achieves firm contact with the adjacent blades under all operating conditions. The reaction force between shrouds can be adjusted by design parameters such as the shroud pitch increment, blade slant angle during assembly, taper angle of the shroud edge, and so on. These design parameters are optimized in the blade design by conducting an FEA sensitivity analysis.

ANALYTICAL METHOD

Analysis of Vibratory Stress Due to Nozzle Wake Excitation Force

In multistage turbomachinery, the interaction between the nozzle and the blades generates an excitation force on the blades, which comes from the wake of the upstream nozzle or the potential field of the upstream/downstream nozzle. The fundamental frequency of the excitation force due to the interaction between the nozzle and the blade is the rotor speed multiplied by the nozzle count. If the natural frequency of the blade coincides with the frequency of the excitation force, the resonant stress of the blade may become very large and may cause a blade failure due to high cycle fatigue (HCF). In mechanical drive steam turbines especially, the resonant stress due to nozzle wake excitation force can cause blade failure, unless the blade and the nozzle are designed properly.

When the bladed disk system of the ISB structure is rotating as shown in Figure 2, the resonant condition and the resonant stress due to nozzle wake excitation force can be expressed by Equation (A-14) and (A-15). The detailed procedure to obtain these equations is described in APPENDIX A.

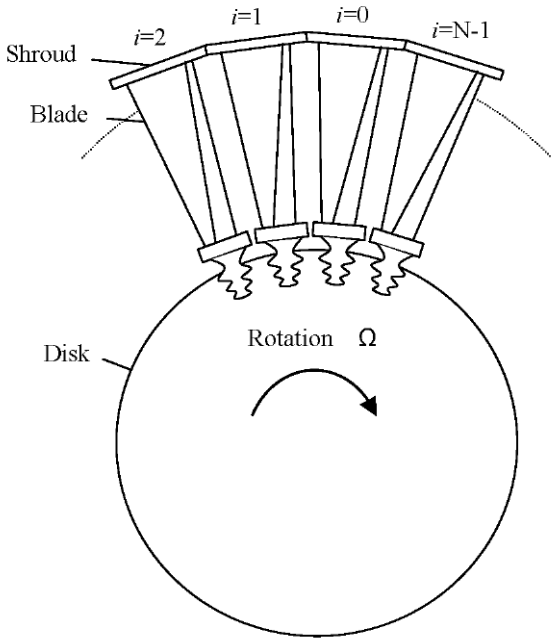

Figure 2. Bladed Disk of ISB Structure.

In calculating the resonant response of the blade due to nozzle wake excitation force, 3D CFD and 3D FEA are used. Figure 3 shows the procedure for calculating the resonant stress of the blade. This method is similar to the ones published in their papers by Chiang and Kielb (1993) and Hilbert, et al. (1997). The resonant stress is calculated as follows:

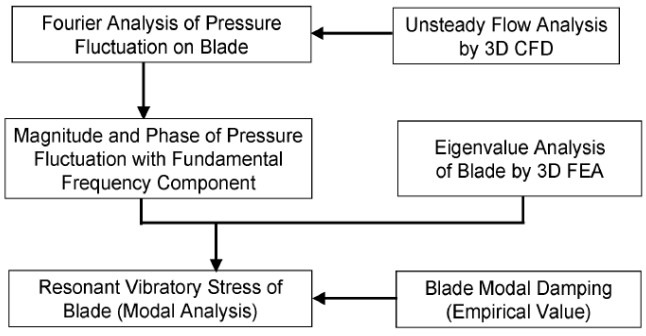

Figure 3. Procedure for Calculating Resonant Stress of Blade.

- The pressure fluctuation on the blade surface is obtained in the form of time-history wave by the blade-vane interaction analysis with unsteady 3D CFD. The magnitude and the phase of the pressure fluctuation with the fundamental frequency (the rotor speed multiplied by the vane count) are calculated by Fourier analysis.

• The eigenvalue analysis of the bladed disk is carried out by 3D FEA, and the resonant stress is calculated by Equation (A-15). The magnitude and the phase of the excitation force on each grid point of the finite element (FE) model are obtained by the pressure fluctuation calculated by 3D CFD, multiplying the pressure fluctuation by the effective area around the grid point. The calculated value or empirical value is used for the blade damping.

When calculating the modal force in a real case, the vibration mode on the CFD mesh or the pressure fluctuation on the FE mesh must be obtained by interpolation, because both meshes are usually different. It is important to note that interpolating the vibration mode of the FE mesh on the CFD mesh makes the calculation error small, because the vibration mode is continuous on the blade surface, while the phase and amplitude of the pressure fluctuation sometimes abruptly change. For this reason, when calculating the modal force, first, the excitation force on CFD mesh is calculated, by multiplying the pressure fluctuation by the effective area. Next, the vibration mode on CFD mesh is obtained by interpolating the vibration mode of the FE mesh. Finally, the modal force is obtained by summing up the product of the vibration mode and excitation force over the blade surface.

Analysis of Vibratory Stress Due to Shock Load

Partial admission has been applied to the control stage of a mechanical drive steam turbine because it produces high turbine efficiency at low loads. Under partial admission conditions, steam is admitted to the rotating blades of a turbine through only a part of the circumference of the stationary row of nozzles. As the rotating blades enter and leave the arc of admission, they receive a rapid load increase and then a rapid load decrease, respectively. The general character of the forces and moments acting on the blades is illustrated in Figure 4 (Pigott, 1980). The shock loads caused by partial admission generate an excitation force on the blade causing it to vibrate. The instant that the blade enters the arc of admission, it begins to vibrate due to the inlet shock. Then the vibration decreases due to damping after it completely enters the arc of admission and the load on it becomes constant. Next, the instant the blade leaves the arc of admission, it receives the exit shock, and then the vibration decreases due to damping during the arc of nonadmission until it enters the next arc of admission. Superimposing the vibration due to the shock load on the residual vibration in this manner, the vibration of the blade becomes steady-state.

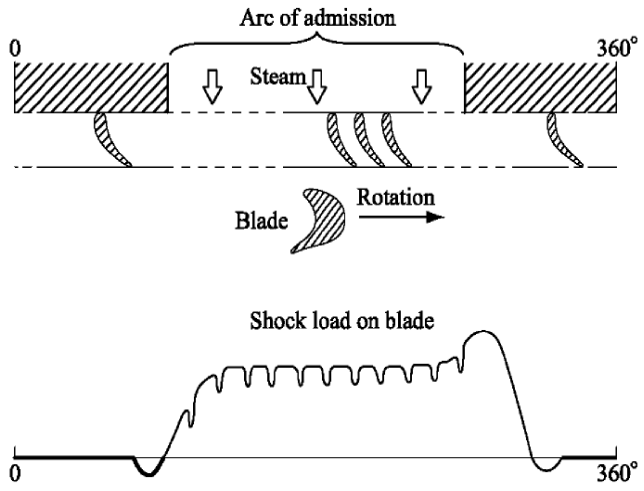

Figure 4. General Character of Blade Forces Due to Shock Load.

The vibratory stress of the blade due to shock load can be calculated by Equation (A-18). The detailed procedure to obtain this equation is described in APPENDIX A.

CALCULATED RESULTS

Vibratory Stress Due to Nozzle Wake Excitation Force

In the ISB structure, the blade is brought into contact with the adjacent blade at the shroud. Because the ISB structure is cyclically symmetric and shows the vibration characteristics of the continuous ring type structure, in the vibration analysis only one blade is modeled, and the eigenvalue analysis of Equation (A-1) is first carried out by use of the cyclic symmetry method. In order to accurately predict the blade frequency and the resonant stress, it is essential to model the geometry of the blade and the shroud precisely. Therefore, usually 3D solid element theory is used in the vibration analysis of the ISB structure. If the stiffness of the disk is much larger than that of the blade like in the last stage of the low-pressure end blades, the FE model of a blade alone can be used. On the other hand, if the stiffness of the blade is comparable with that of the disk like a blade in the upstream stage, the FE model of a bladed disk should be used.

Table 1 shows the specification of the intermediate stage blade of the mechanical steam turbine used in the analysis, and Figure 5 gives the 3D FE model of the blade. Figure 6 and Figure 7 show the calculated natural frequencies and Campbell diagram of the blade, respectively. The two zigzag lines in Figure 6 are what are called interference lines corresponding to the maximum and minimum operating speed. Only vibration modes of the bladed disk where the interference lines in Figure 6 cross the curves of natural frequencies will respond to the harmonic excitation force in the range of the operation speeds. The frequency curves in Figure 7 seem to be very complicated, because only the resonant points that satisfy Equation (A-14) are plotted and connected. By use of Figure 6 and Figure 7, a blade designer can easily identify dangerous vibration modes that can respond to the harmonic excitation force in the operating speed range.

Table 1. Characteristics of Intermediate Stage Blade.

Min. Speed	7500 rpm
Max. Speed	9500 rpm
Blade Height	20 mm
Blade Count	76
Nozzle Count	86

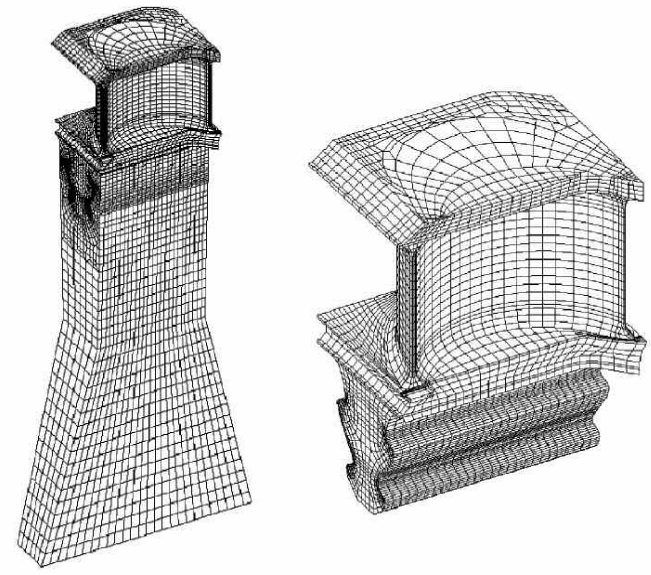

Figure 5. 3D FE Model of Intermediate Stage Blade.

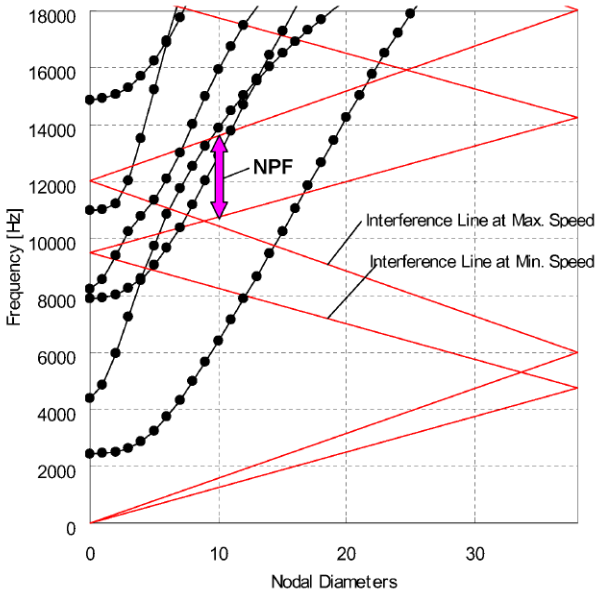

Figure 6. Natural Frequency of Intermediate Stage Blade.

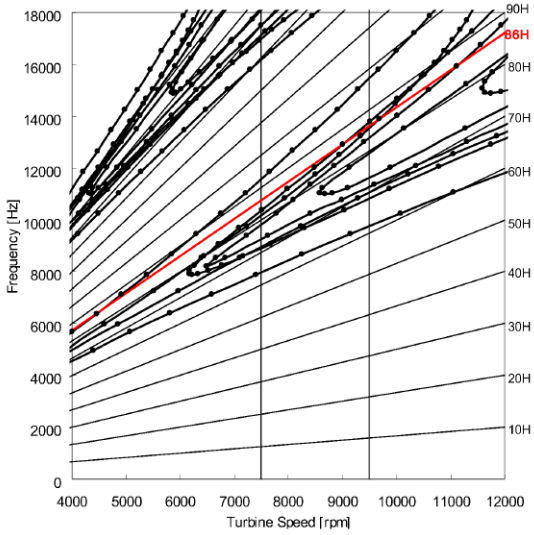

Figure 7. Campbell Diagram of Intermediate Stage Blade.

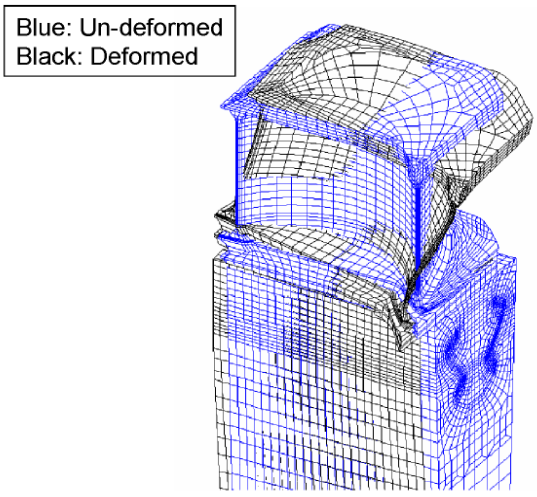

Figure 8. Vibration Mode of Intermediate Stage Blade.

Since the blade count used in the analysis from Table 1 is 76, and the harmonic index of the special excitation force (the upstream vane count) is 86, only a vibration mode with n = 10 can respond to the nozzle wake excitation force from Equation (A-14). Therefore, the analysis of the resonant stress due to the nozzle wake excitation force is carried out, and only the vibration modes with n = 10 are shown in Figure 6, considering the prediction error of the natural frequency. Figure 8 illustrates the vibration modes with n = 10, which is an axial bending mode.

Figure 9 shows the 3D CFD mesh, which consists of the upstream vane and the blade. Figure 10 and Figure 11 show the typical results of CFD analysis. Figure 10 shows the entropy distribution. In Figure 10, the red part corresponds to the wake, which induces the pressure fluctuation on the blade. Figure 11 shows the magnitude and the phase of the pressure fluctuation on the blade with blade passing frequency, which was obtained from a Fourier analysis of the time-history wave of the pressure fluctuation. By using these results, the resonant stress for the nozzle wake excitation was calculated according to the procedure in Figure 3. Finally, the safety factor to HCF was evaluated by use of the calculated steady and resonant stress and Goodman diagram of the material as shown in Figure 12. It can be said that all vibration modes that can respond to the nozzle wake excitation force have a large enough safety factor.

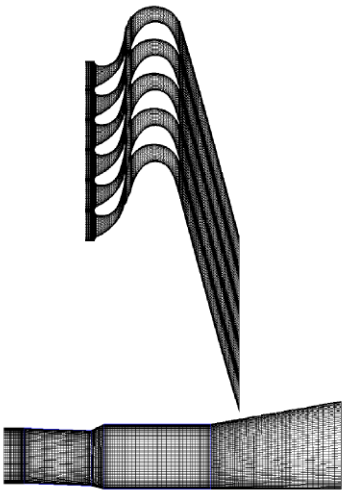

Figure 9. 3D CFD Mesh for Calculating Stage Interaction Force.

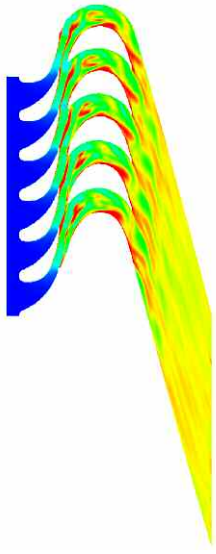

Figure 10. Example of Entropy Distribution (50 Percent Height Section).

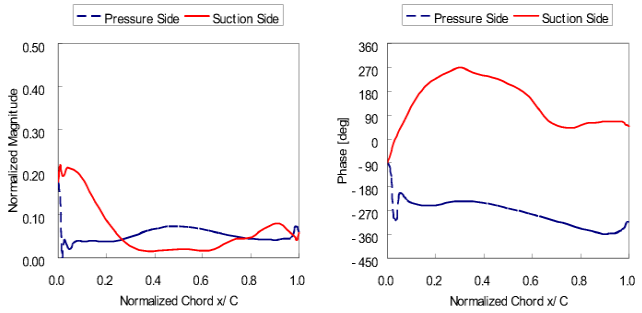

Figure 11. Magnitude and Phase of Pressure Fluctuation with Blade Passing Frequency (50 Percent Height Section).

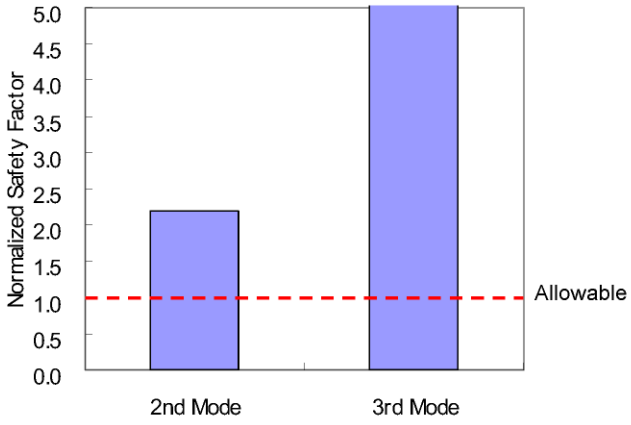

Figure 12. Safety Factor to HCF.

Vibratory Stress Due to Shock Load

Table 2 shows the specification of the control stage blade of the mechanical steam turbine used in the analysis of the vibratory stress due to shock load. In order to make a comparison of the mechanical strength, the analysis was carried out for the ISB structure and the conventional grouped blades structure. Except for the geometry of the tenon and shroud, the geometry of the blade profile and the vane count are the same in both structures.

Table 2. Characteristics of Control Stage Blade.

Blade Height	20 mm
Rated speed	6870 - 9610 rpm
Blade count	52
Nozzle count	113

Figure 13 shows the 3D FE model of the blades. Figure 14 and Figure 15 show the results of CFD analysis for the condition of 25 percent admission, where the steam is admitted to the rotating blades of a turbine through a quarter of the circumference of the stationary row of nozzles. Figure 14 shows the total pressure distribution. In Figure 14, the bluish-green color corresponds to the high-pressure region, while the blue part corresponds to the low-pressure region. This pressure distribution induces a shock load on the blade. Figure 15 shows the typical shock load on the blade (pressure fluctuation around the leading edge). As shown in Figure 15, the pressure on the blade clearly changes in the range of the admission and nonadmission regions, and the blade receives a shock load close to a square wave as pointed out in experimental studies conducted by Fridh, et al., 2004. The component of high frequency in Figure 15 corresponds to the nozzle wake excitation frequency, which is the rotor speed multiplied by vane count (113).

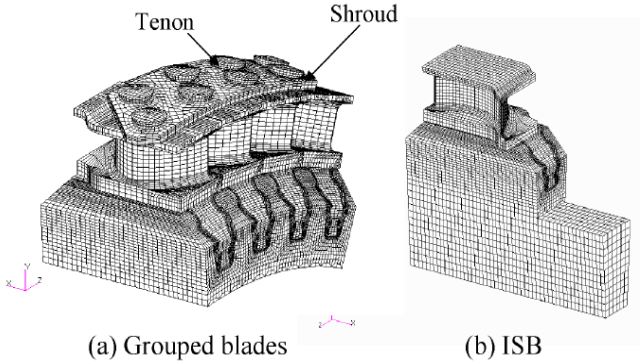

Figure 13. 3D FE Model of Control Stage Blade.

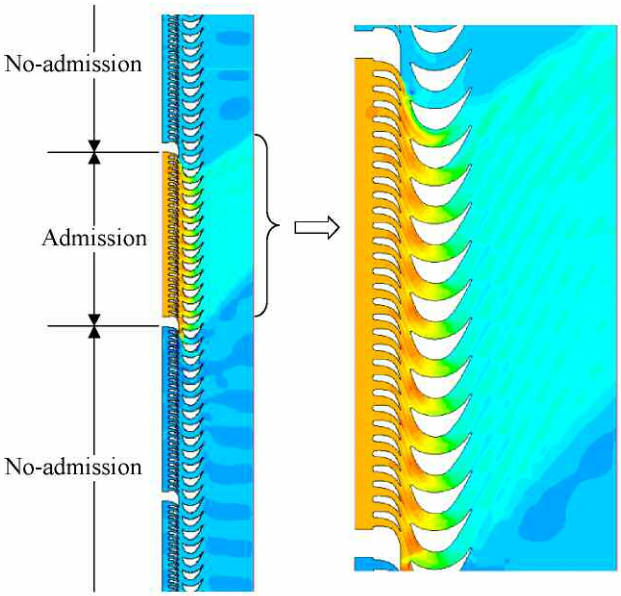

Figure 14. Total Pressure Distribution Calculated by CFD (25 Percent Admission).

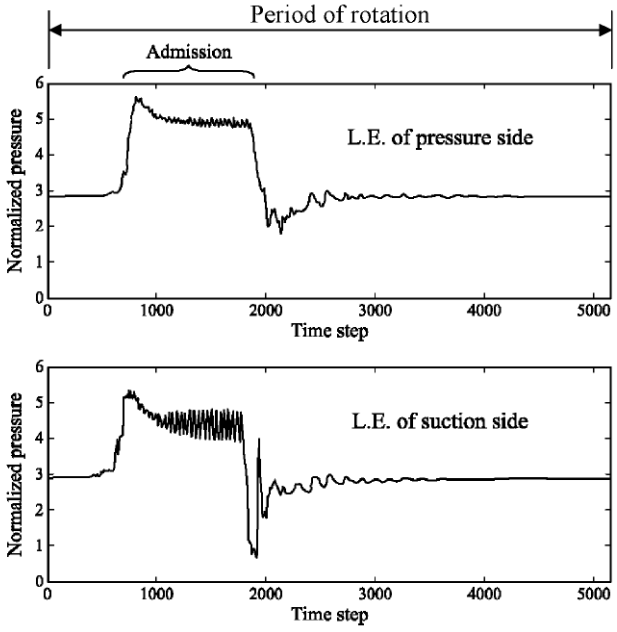

Figure 15. Pressure Fluctuation on the Blade Calculated by CFD (25 Percent Admission).

Figure 16 shows the relative safety factors of the ISB and grouped blades structure for the shock loads due to partial admission. In Figure 16, the safety factors were evaluated for the condition of 25 percent and 75 percent admission by use of the calculated steady and vibratory stress and the Goodman diagram of the material. The damping of both structures are assumed to be identical, and about 10 vibration modes were used to calculate the vibratory stress. It can be said that the mechanical strength of the ISB structure is superior to that of the grouped blade structure. As expected, the tenon decreases the mechanical strength of the grouped blades structure.

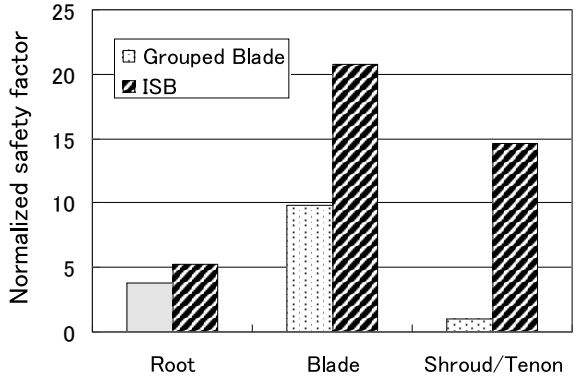

Figure 16. Comparison of Safety Factor of ISB and Grouped Blade.

VERIFICATION OF ANALYSIS METHOD

Natural Frequency of a Bladed Disk

In order to confirm the vibratory characteristics of the advanced ISB structure, a rotating vibratory test was carried out, using a high-speed balance facility (Sasaki, et al., 2002). The measured natural frequencies were compared with the calculated frequencies. A test rotor consisting of three stages of ISB structures was set up in a vacuum chamber of the high-speed balance facility. During the test, the rotor speed was gradually changed and the blades were excited by the air-jet to completely measure the resonating stress. The natural frequencies of the blades were measured by a conventional telemetry system with strain gauges.

Figure 17 shows the test rotor used in the rotating vibratory test and Figure 18 shows the typical Campbell diagram measured in the test. Although the measured vibratory stress is very low, the Campbell diagram shows the typical vibratory characteristics of the ring type structure. Figure 19 shows the comparison of the calculated and measured natural frequency of the ISB. From the result, it can be seen that the natural frequency of the ISB can be predicted by FEA with practical accuracy.

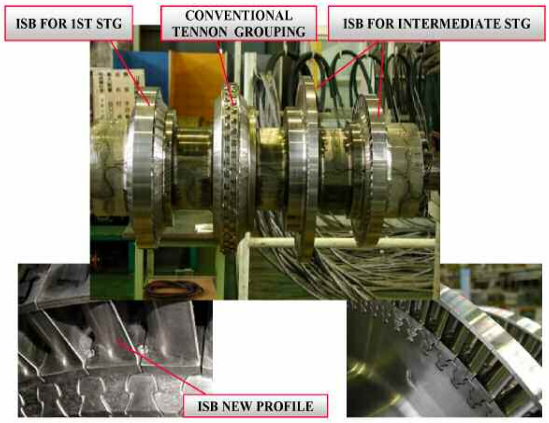

Figure 17. Rotating Vibratory Test Rotor.

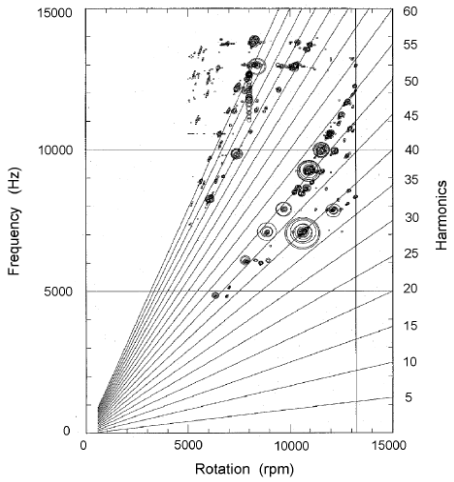

Figure 18. Typical Campbell Diagram Measured in Rotating Vibratory Test.

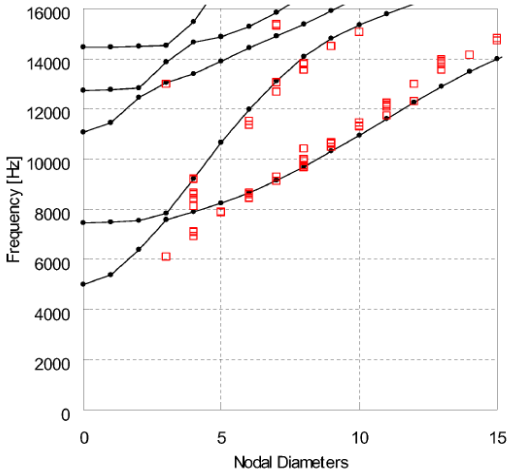

Figure 19. Comparison of Calculated and Measured Natural Frequencies of ISB.

Vibratory Stress

Many tests were conducted by the authors to verify the validity of their own analysis methods for vibratory stresses caused by nozzle wake excitation forces. These tests compared the measured vibratory stress with the calculated stress for the blades of industrial gas turbines and steam turbines (Kaneko, et al., 2006). From the results of the verification tests, it was confirmed that the vibratory stress caused by the nozzle wake excitation force can be predicted by the analysis described in this paper.

To further verify the results a test was conducted on a turbine stage of a turbocharger, which consists of a vane followed by a blade. Strain gauges were attached to the blades, and the vibratory stresses of the blades resonating with the nozzle wake excitation force were measured by use of a telemetry system. Table 3 shows the specification of the measured blade. In the test, the rotor speed was gradually changed to completely measure the resonating stress and damping. Figure 20 shows the vibration modes calculated by FEA. Figure 21 shows the CFD mesh, which consists of the first stage vane and blade. Figure 22 shows the magnitude and the phase of the pressure fluctuation on the first stage blade caused by the blade passing frequency, which was obtained from a Fourier analysis of the time-history wave of the pressure fluctuation calculated by CFD. Figure 23 shows the comparison of the measured and calculated results. As shown in Figure 23, the resonant stresses calculated by the procedure described in this paper show good agreement with the measured results.

Table 3. Characteristics of Measured Blade.

Blade Height	143 mm
Rated speed	8500 - 9000 rpm
Blade count	35
Nozzle count	23

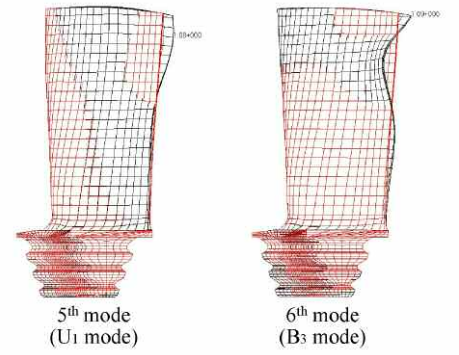

Figure 20. Vibration Modes of Tested Blade.

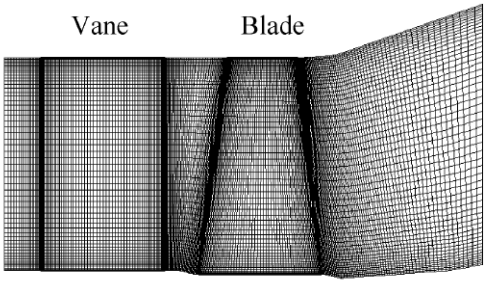

Figure 21. 3D CFD Mesh for Tested Blade.

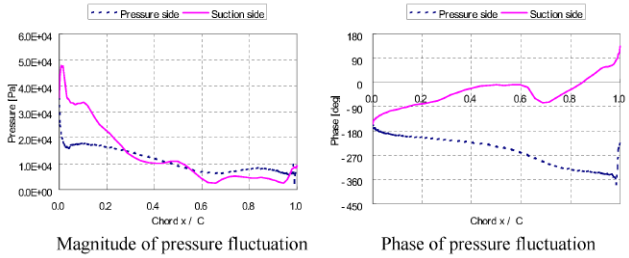

Figure 22. Magnitude and Phase of Pressure Fluctuation on Blade.

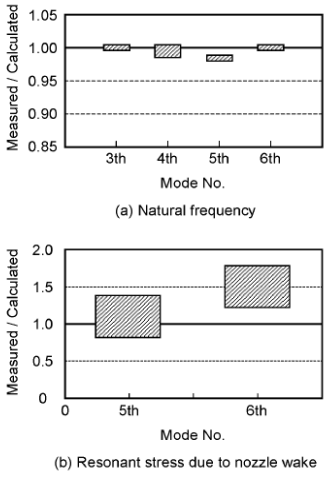

Figure 23. Comparison of Measured and Calculated Resonant Stress.

As for the vibratory stress caused by the shock load due to partial admission operation, no verification test for an actual turbine has been done so far, but will be carried out in the near future.

FIELD EXPERIENCE

Since the first application of the advanced ISB in 2001, more than 60 turbines have been designed and are operating in the field successfully. Figure 24 indicates the field experience of these turbines compared with other conventional design turbines. The advanced ISB is applied especially on synthesis gas compressor drive steam turbines that require high stage power with large steam flow and high rotational speed. In order to achieve high efficiency and integrity for each severe operating condition, the blade design has been optimized by the use of the advanced ISB structure, which has been in this paper.

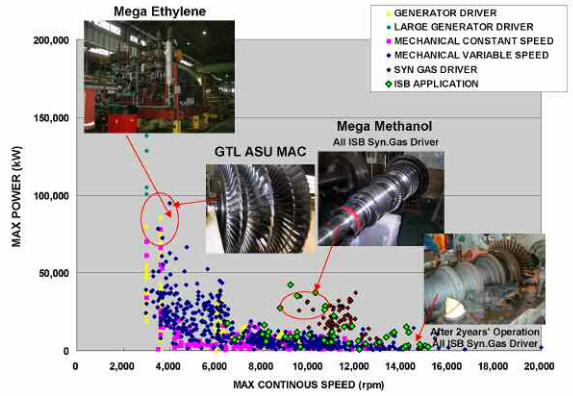

Figure 24. Application and Field Experience of ISB.

Figure 25 shows a typical mechanical drive turbine of 37,000 kW using the advanced ISB for the world's largest ammonia plant. High-pressure inlet steam flow and exhaust steam flow are 380 ton/h and 120 ton/h, respectively, when rotating at the maximum speed of 10,274 rpm. Currently, a steam turbine of over 40,000 kW for a synthesis gas compressor drive that was designed utilizing the same technology is under commissioning.

Figure 25. Typical ISB Applied to Mechanical Drive Turbine (After Operation).

CONCLUSION

An advanced ISB structure has been developed for use in the control stage and intermediate stage of mechanical drive steam turbines in order to improve reliability and thermal efficiency. This paper described the analysis method, the calculated results, and verification test results used for the design of the advanced ISB structure. From these results, the authors confirmed that the

vibration characteristics of the continuously coupled blade using the advanced ISB structure can be predicted for the intermediate and the control stage. It has also been further shown that the use of a tenon decreases the mechanical strength of the grouped blades structure and that the mechanical strength of the ISB structure is superior.

The advanced ISB structure has been successfully operating in the field since the first application in 2001. Hereafter, the advanced ISB structure will be applied not only for new turbines but also for any existing turbine refurbishment to improve the efficiency and the reliability.

APPENDIX A

Derivation of the Vibratory Stresses
Due to the Nozzle Wake Excitation Force

The vibration response of the blade to the interaction force between the nozzle and the blade can be analyzed, as well as the lower frequency excitation force generated from the flow distortion caused in the circumferential direction. When the bladed disk system of the ISB structure is rotating in the circumferentially nonuniform flow, the equation of motion for the bladed disk system in Figure 2 can be expressed by Equation (A-1):

$$[M_T]\{\ddot{U}_{T,H}\}+[K_T]\{U_{T,H}\}=\{P_{T,H}\} \tag{A-1}$$

Where $[M_T]$, $[K_T]$, $\{U_{T,H}\}$, and $\{P_{T,H}\}$ are the mass matrix, stiffness matrix, displacement vector and excitation force vector of the whole bladed disk system, and can be expressed by Equation (A-2):

$$[M_T]=\begin{bmatrix}[M] & & & 0\\ & [M] & & \\ & & \ddots & \\ 0 & & & [M]\end{bmatrix}\ (Cyclic\ matrix)$$

$$[K_T]=\begin{bmatrix}[K_1] & [K_2] & [0] & \cdots & [K_2]^T\\ [K_2]^T & [K_1] & [K_2] & & \\ 0 & [K_2]^T & [K_1] & & \\ & & & \ddots & \\ & & & & [K_1]\end{bmatrix}\ (Cyclic\ matrix)$$

$$\{U_{T,H}\}^T=\{\{U_{0,H}\}^T\{U_{1,H}\}^T\cdots\cdots\{U_{N-1,H}\}^T\}$$

$$\{P_{T,H}\}^T=\{\{P_H\}^T\cos(\omega t-\gamma_H)\ \{P_H\}^T\cos(\omega t-\gamma_H-\alpha_H)\ \cdots\cdots\{P_H\}^T\cos(\omega t-\gamma_H-(N-1)\alpha_H)\} \tag{A-2}$$

In Equation (A-2), [M] and $[K_1]$ are the mass matrix and the stiffness matrix of a substructure containing one blade, and $[K_2]$ is the stiffness matrix determined by the boundary condition between the adjacent blades, and $\{U_{i,H}\}$ is the displacement vector of the i-th blade. $\{P_H\}$ and γ_H are the amplitude and the phase of the excitation force acting on the blade, while ω is the angular frequency, and α_H is the phase angle caused by the rotation of the bladed disk system. The subscript T and H refer to the whole bladed disk system and the harmonic index of the excitation force, respectively.

Let the angular speed of the rotor be Ω, the excitation harmonic (engine order) be H, and the number of the blades in the bladed disk system be N, then ω and α_H can be expressed by Equation (A-3):

$$\omega=H\Omega,\quad \alpha_H=\frac{2\pi H}{N} \tag{A-3}$$

Although the detailed procedure to obtain the solution of Equation (A-1) is not shown, applying the cyclic symmetry method and the modal analysis method, and introducing the modal damping to Equation (A-1), the response of the blade to the excitation force of engine order H can be expressed by Equation (A-4) (Kaneko, et al., 2003):

$$\{U_{T,H}(t)\}=\sum_{m=1}^{M}\left(p_m(t)\{\Psi_{n1}^m\}+q_m(t)\{\Psi_{n2}^m\}\right) \tag{A-4}$$

$$\left.\begin{aligned}p_m(t)&=\left(P_1^m X_c^m+P_2^m X_s^m\right)\cos(\omega t-\gamma_H)\\&\quad+\left(P_1^m X_s^m-P_2^m X_c^m\right)\sin(\omega t-\gamma_H)\\ q_m(t)&=\left(P_2^m X_c^m-P_1^m X_s^m\right)\cos(\omega t-\gamma_H)\\&\quad+\left(P_2^m X_s^m+P_1^m X_c^m\right)\sin(\omega t-\gamma_H)\end{aligned}\right\} \tag{A-5}$$

$$\left.\begin{aligned}X_c^m&=\frac{1-\beta_m^2}{\left(1-\beta_m^2\right)^2+\left(2\varsigma_m\beta_m\right)^2}\frac{1}{M_m\omega_m^2}\\ X_s^m&=\frac{2\varsigma_m\beta_m}{\left(1-\beta_m^2\right)^2+\left(2\varsigma_m\beta_m\right)^2}\frac{1}{M_m\omega_m^2}\\ \beta_m&=\frac{\omega}{\omega_m}\end{aligned}\right\} \tag{A-6}$$

$$M_m=\{\phi_{nR}^m\}^T[M]\{\phi_{nR}^m\}+\{\phi_{nI}^m\}^T[M]\{\phi_{nI}^m\} \tag{A-7}$$

$$P_1^m=\{\phi_{nR}^m\}^T\{P_H\},\quad P_2^m=\{\phi_{nI}^m\}^T\{P_H\} \tag{A-8}$$

Where ω_m is the natural frequency of the bladed disk, and ζ_m is the modal damping ratio. The vector $\{\phi_{nR}^m\}$ and $\{\phi_{nI}^m\}$ are the real and imaginary modes obtained from eigenvalue Equation (A-1), if the right-hand side is replaced by zero. The subscript n and m refer to the harmonic index (the number of nodal diameters in a broad sense) and the order of vibration mode, respectively. $\{\Psi_{n1}^m\}$and $\{\Psi_{n2}^m\}$ are column vectors whose elements consist of the eigenvectors of blades arranged in order of blade number as Equation (A-9):

$$\left.\begin{aligned}\{\Psi_{n1}^m\}^T&=\{\{\phi_{nR}^m\}^T\left(\cos\alpha_n\{\phi_{nR}^m\}^T-\sin\alpha_n\{\phi_{nI}^m\}^T\right)\\&\quad\cdots\left(\cos(N-1)\alpha_n\{\phi_{nR}^m\}^T-\sin(N-1)\alpha_n\{\phi_{nI}^m\}^T\right)\}\\ \{\Psi_{n2}^m\}^T&=\{\{\phi_{nI}^m\}^T\left(\cos\alpha_n\{\phi_{nI}^m\}^T+\sin\alpha_n\{\phi_{nR}^m\}^T\right)\\&\quad\cdots\left(\cos(N-1)\alpha_n\{\phi_{nI}^m\}^T+\sin(N-1)\alpha_n\{\phi_{nR}^m\}^T\right)\}\end{aligned}\right\} \tag{A-9}$$

As is well known, in the structure of cyclic symmetry like the ISB, all other relationships between H and n except for $H \pm n = \lambda N$ (λ: any integer) result in the zero response in the n-th mode harmonic because the modal force is cancelled over the whole bladed disk. Therefore, it is sufficient that the only eigenvectors satisfying the equation of $H \pm n = \lambda N$ are summed in Equation (A-4). In the resonance ($\omega = \omega_m$), Equation (A-10) is derived from Equation (A-6):

$$X_c^m=0,\quad X_s^m=\frac{1}{2\varsigma_m}\frac{1}{M_m\omega_m^2},\quad \beta_m=1 \tag{A-10}$$

Substituting Equation (A-10) into Equation (A-4) and Equation (A-5), the resonant response of the bladed disk can be written as Equation (A-11):

$$\begin{aligned}\{U_{T,H}(t)\} = {} & X_s^m\left(P_2^m\{\Psi_{n1}^m\} - P_1^m\{\Psi_{n2}^m\}\right)\cos(\omega t - \gamma_H) \\ & + X_s^m\left(P_1^m\{\Psi_{n1}^m\} + P_2^m\{\Psi_{n2}^m\}\right)\sin(\omega t - \gamma_H)\end{aligned} \quad \text{(A-11)}$$

From Equation (A-9) and Equation (A-11), the resonant response of the k-th blade can be expressed as Equation (A-12) and Equation (A-13):

$$\{U_{k,H}(t)\} = \frac{1}{2\varsigma_m}\frac{1}{M_m\omega_m^2}\left[\{A\}\cos(\omega t - \gamma_H - k\alpha_H) + \{B\}\sin(\omega t - \gamma_H - k\alpha_H)\right] \quad \text{(A-12)}$$

$$\left.\begin{aligned}\{A\} &= \{\phi_{nI}^m\}^T\{P_H\}\{\phi_{nR}^m\} - \{\phi_{nR}^m\}^T\{P_H\}\{\phi_{nI}^m\} \\ \{B\} &= \{\phi_{nI}^m\}^T\{P_H\}\{\phi_{nI}^m\} + \{\phi_{nR}^m\}^T\{P_H\}\{\phi_{nR}^m\}\end{aligned}\right\} \quad \text{(A-13)}$$

From Equation (A-12), it can be said that the traveling wave mode is excited in the resonance of the ISB structure. In other words, the requisite equation for the resonance of the ISB structure is expressed by Equation (A-14), and if the negative sign in Equation (A-14) is satisfied, the backward traveling wave, whose nodal diameters move in the opposite direction to that of the rotation of the rotor, is excited. Conversely, if the positive sign is satisfied, the forward traveling wave is excited. The resonant amplitudes of all blades are identical but the phase is different by α_H between adjacent blades.

$$\omega = \omega_m, \quad H \pm n = \lambda N \quad \text{(A-14)}$$

Equation (A-12) is the expression for the resonant displacement. Equation (A-15) and Equation (A-16) for the resonant stress can be obtained in the same manner, replacing $\{\phi_{nR}^m\}$ and $\{\phi_{nI}^m\}$ in Equation (A-4) by the stress mode $\{\sigma_{nR}^m\}$ and $\{\sigma_{nI}^m\}$:

$$\{\sigma_{k,H}(t)\} = \frac{1}{2\varsigma_m}\frac{1}{M_m\omega_m^2}\left[\{A_\sigma\}\cos(\omega t - \gamma_H - k\alpha_H) + \{B_\sigma\}\sin(\omega t - \gamma_H - k\alpha_H)\right] \quad \text{(A-15)}$$

$$\left.\begin{aligned}\{A_\sigma\} &= \{\phi_{nI}^m\}^T\{P_H\}\{\sigma_{nR}^m\} - \{\phi_{nR}^m\}^T\{P_H\}\{\sigma_{nI}^m\} \\ \{B_\sigma\} &= \{\phi_{nI}^m\}^T\{P_H\}\{\sigma_{nI}^m\} + \{\phi_{nR}^m\}^T\{P_H\}\{\sigma_{nR}^m\}\end{aligned}\right\} \quad \text{(A-16)}$$

Derivation of the Vibratory Stress Due to Shock Load

The shock load on a blade can be calculated by the stage interaction analysis between the blades and vanes, where all of the blades and vanes over 360 degrees are analyzed by CFD. The calculated time history waves of the shock loads are expanded into Fourier series, and decomposed into the harmonic excitation forces as expressed in Equation (A-17), in order to calculate the vibratory stress under steady condition:

$$\left.\begin{aligned}F_i(t) &= \frac{a_{i,0}}{2} + \sum_{H=1}^{\infty}\left(a_{i,H}\cos H\Omega t + b_{i,H}\sin H\Omega t\right) \\ &= \frac{a_{i,0}}{2} + \sum_{H=1}^{\infty} P_{i,H}\cos(\omega t - \gamma_{i,H}) \\ P_{i,H} &= \sqrt{a_{i,H}{}^2 + b_{i,H}{}^2}, \quad \gamma_{i,H} = \tan^{-1}\frac{b_{i,H}}{a_{i,H}}\end{aligned}\right\} \quad \text{(A-17)}$$

Where $F_i(t)$ is the shock load acting on the i-th grid point of the first blade on a bladed disk. $P_{i,H}$ and $\gamma_{i,H}$ are the amplitude and the phase of the harmonic components of the shock load, and is used as the phase of the harmonic excitation force in Equation (A-2). The steady vibration due to the shock load can be obtained by superposing the responses to the harmonic excitation forces of Equation (A-17) in the time domain, which is calculated by Equation (A-15).

When calculating the vibratory stress in blade design, the probable resonant modes under rated speed are selected from Equation (A-14), and the resonant response is then calculated assuming that these modes are completely resonant ($\beta_m = 1$). Second, the resonant response to each harmonic excitation force is superimposed in the time domain, and the response to the shock load is calculated as Equation (A-18):

$$\{U_T^S(t)\} = \sum_{H=1}^{H_{max}}\{U_{T,H}(t)\} \quad \text{(A-18)}$$

The response to the shock load used in the blade mechanical design is defined as the maximum value of Equation (A-18).

REFERENCES

Chiang, H. D. and Kielb, R. E., 1993, "An Analysis System for Blade Forced Response," *Journal of Turbomachinery, 115,* pp. 762-770.

Fridh, J. E., Bunkute, B., Fakhrai, R., and Fransson, T. H., 2004, "An Experimental Study on Partial Admission in a Two-Stage Axial Air Test Turbine with Numerical Comparisons," ASME GT-2004-53774, pp. 1-13.

Hilbert, G. R., Ni, R. H., and Takahashi, R. K., 1997, "Forced Response Prediction of Gas Turbine Rotor Blades," ASME Winter Annual Meeting.

Ikeno, K., Nagai, N., Hirano, Y., and Sasaki, T., 2004, "Application of Advanced Integral Shrouded Blades to High-Speed and High-Power Mechanical Drive Steam Turbine," Mitsubishi Heavy Industries, Ltd., Technical Review, *41,* (3), pp. 1-6.

Kaneko, Y., Mori, K., and Tochitani, N., 2003, "Analysis and Measurement of Resonant Vibratory Stress of Integral Shroud Blade for Steam Turbine," Proceedings of the International Conference on Power Engineering-03 (ICOPE-03), *2,* pp. 189-194.

Kaneko, Y., Mori, K., Yamashita, H., and Sato, K., 2006, "Analysis of Variation of Natural Frequency and Resonant Stress of Blade," ASME GT-2006-90176, pp. 1-7.

Pigott, R., 1980, "Turbine Blade Vibration Due to Partial Admission," International Journal of Mechanical Science, 22, pp. 247-264.

Sasaki, T., Hata, S., and Ikeno, K., 2002, "New Technologies of Synthesis Gas Compressor Drive Steam Turbines for Increasing Efficiency and Reliability," *Proceedings of the Thirty-First Turbomachinery Symposium,* Turbomachinery Laboratory, Texas A&M University, College Station, Texas, pp.75-83.